

Relationship between Pairing Symmetries and Interaction Parameters in Iron-Based Superconductors from Functional Renormalization Group Calculations

Jing Yuan¹ and Jiangping Hu^{1,2,3}

¹*Institute of Physics, Chinese Academy of Sciences, Beijing 100190, China*

²*Department of Physics, Purdue University, West Lafayette, Indiana 47907, USA*

³*Collaborative Innovation Center of Quantum Matter, Beijing, China*

(Dated: November 7, 2018)

Pairing symmetries of iron-based superconductors are investigated systematically in a five-orbital model within the different regions of interaction parameters by functional renormalization group(FRG). Even for a fixed Fermi surface with both hole and electron pockets, it is found that depending on interaction parameters, a variety of pairing symmetries, including two types of d -wave and two types of s -wave pairing symmetries, can emerge. Only the $d_{x^2-y^2}$ and the s_{\pm} waves are robustly supported by the nearest-neighbor(NN) intra-orbital J_1 and the next-nearest-neighbor(NNN) intra-orbital J_2 antiferromagnetic(AFM) exchange couplings respectively. This study suggests that the accurate initial input of interaction parameters are essential to make FRG an useful method to determine the leading channel of superconducting instability.

PACS numbers: 74.70.Xa, 74.20.-z, 74.20.Rp, 74.25.Dw

I. INTRODUCTION

The discovery of high temperature Fe-based superconductors(FeSCs) is a major breakthrough in condensed matter physics field¹. Since their great application prospect, lots of theoretical and experimental researches have been devoted to study the FeSCs²⁻⁸. There is an increasing diversity of superconducting materials and more complicated characteristics. Nevertheless, the mechanism of FeSCs has not been confirmed thoroughly.

Iron-pnictides usually contain both hole and electron pockets which are separated with momentum (π, π) in 2-Fe Brillouin zone(BZ). Theoretically, s_{\pm} -wave^{2,9-11}, which displays a sign change between the superconducting orders on hole pockets and electron pockets, is the most promising candidate. However, once the Fermi surfaces change, s_{\pm} is not the leading instability in many theoretical studies. For example, in the FeSCs with only electron pockets, such as most iron-chalcogenides¹²⁻¹⁴, or only hole pockets¹⁵⁻¹⁷, the d -wave pairing channel is favored in most theoretical studies based on spin fluctuation mechanism and standard weak coupling treatments¹⁷⁻²⁰. In addition, orbital dependent sign change s -wave^{21,22}, s_{\pm}^h ^{20,23,24} with sign-reversal between hole pockets, η -pairing s -wave²⁵ and time-reversal symmetry breaking states including $s + id$ state^{26,27} and $s + is$ state^{28,29} have been proposed theoretically.

While most weak coupling approaches have targeted on the change of pairing symmetries depending on the variations of Fermi surfaces, the relationship between interaction parameters and pairing symmetries has not been well explored. In our paper based on functional renormalization group(FRG)³⁰⁻³⁴, an unbiased weak coupling approach, we systematically investigate the effect of interaction parameters on pairing symmetries in a fixed Fermi surface topology that exhibits both hole and electron pockets³⁵. We consider interactions including

intra-orbital Coulomb coupling U , inter-orbital Coulomb coupling U' , Hund's coupling J_H , pairing hopping term J_{pair} , nearest-neighbour(NN) antiferromagnetic(AFM) exchange coupling J_1 , and next-nearest-neighbour(NNN) AFM exchange coupling J_2 . We calculate the phase diagrams of the leading superconducting instability. It is found that depending on interaction parameters, all s_{\pm} , $d_{x^2-y^2}$, d_{xy} , and s_{\pm}^h phases can be emerged within the reasonable interaction regions. This result suggests that the theoretical predicting power from this current theoretical method is rather limited as it is difficult to extract accurate effective microscopic interaction parameters for complex systems such as iron-based superconductors.

II. METHOD AND MODEL

We use the FRG method to analyze the pairing symmetry with different types of interactions. FRG is a numerical calculation method for weak to moderate electron correlation systems. As it takes into account all virtual two-electron scattering processes and calculates all the electronic instabilities without bias, FRG is considered to be a resultful method in calculating the instabilities and pairing symmetries of materials.

The results of FRG are known to be sensitive to Fermi surface topology and the details of Fermi surfaces properties. Moreover, these results also closely rely on the initial type and value of interactions, which is the central focus of this paper. For the sake of convenience of numerical calculation, we discretize the momenta by dividing the BZ into N patches^{36,37}, here $N = 80$, and each patch contains one Fermi surface segment. So in the numerical process, we treat the particle momentum with the patch index. Approximately, we regard the coupling function as a constant in each patch and ignore the frequency dependence of the vertex function and the self-energy^{38,39}. More specifically, FRG mainly outputs the effective inter-

action as the momentum continually tends to the Fermi surface. The form of four-particle effective interaction is

$$V_{\Lambda}(k_1, k_2, k_3, k_4)c_{k_1 b_1 \alpha}^{\dagger} c_{k_2 b_2 \beta}^{\dagger} c_{k_4 b_4 \beta} c_{k_3 b_3 \alpha}, \quad (1)$$

where $V(k_1, k_2, k_3, k_4)$ exhibits a four-point interaction vertex with the incoming and outgoing momenta k_1, k_2, k_3, k_4 , here we label these particles with the discrete Fermi surface patches; b_1, b_2, b_3, b_4 denote the corresponding band indexes of the four particles and α, β are spin indexes. The energy cutoff Λ is the FRG flow parameter which makes the energy finally approach around the Fermi surface. Apparently, for the superconducting channel $\mathbf{k}_1 = -\mathbf{k}_2 = \mathbf{k}$, $\mathbf{k}_3 = -\mathbf{k}_4 = \mathbf{p}$ and the four-point function becomes $V_{SC}(\mathbf{k}, -\mathbf{k}, \mathbf{p}, -\mathbf{p})$. We rewrite the function into eigen-mode,

$$V_{\Lambda, SC}(\mathbf{k}, -\mathbf{k}, \mathbf{p}, -\mathbf{p}) = \sum_i w_i(\Lambda) f_i^*(\mathbf{k}) f_i(\mathbf{p}), \quad (2)$$

where i is the decomposition index. The leading instability of the superconducting channel corresponds to the eigenvalue $w_1(\Lambda)$ which is the most diverging one as the decreasing of Λ , and the homologous form factor $f_1(k)$ tells us the detailed information of superconducting order parameter, the pairing symmetry and the gap structure.

We adopt the band structure of the optimally doped 122-iron-pnictides. The band structure is described by a five-orbital tight-binding model³⁵,

$$H_0 = \sum_{\mathbf{k}, \sigma} \sum_{a, b=1}^5 (\xi_{ab}(\mathbf{k}) + \epsilon_a \delta_{ab}) c_{a\sigma}^{\dagger}(\mathbf{k}) c_{b\sigma}(\mathbf{k}), \quad (3)$$

where a, b stand for the five Fe d orbitals, σ stands for spin, $\xi_{ab}(\mathbf{k})$ is the kinetic term, ϵ is the onsite energy, $c_{a\sigma}^{\dagger}(\mathbf{k})$ creates an electron with spin σ and momentum \mathbf{k} in orbital a . The parameters used in Eq.3 can be found in Graser's work³⁵. Throughout the rest of this paper, we take the 0.317 hole doping. The band structure and the BZ division are shown in Fig.1. There are three bands crossing Fermi level which forms five Fermi surfaces: two hole pockets centered at $(0, 0)$, one hole pocket centered at (π, π) , and two electron pockets centered at $(\pi, 0)/(0, \pi)$. More details of the model and FRG calculation can be found in our former work⁴⁰.

The total Hamiltonian is given by $H = H_0 + H_I$, where H_I describes effective electron-electron interactions. In the following sections, we will discuss the superconducting pairing symmetry under a different kind of interactions.

III. ONSITE REPULSIVE COULOMB INTERACTION

In this section, we concentrate on the onsite interactions which include the intra- and inter-orbital Coulomb

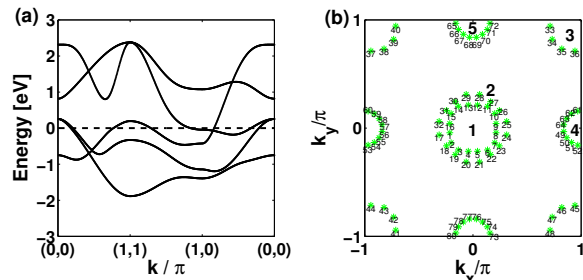


FIG. 1: (color online)(a) The band structure of the five-orbital tight-binding model with chemical potential $\mu = -0.20$ with 0.317 hole doping per Fe atom. (b) Brillouin zone division graph with $N = 80$: the discrete green stars labeled with numbers are the crossing points of patch center lines and Fermi surfaces.

coupling U and U' , Hund's coupling J_H , and pairing hopping term J_{pair} . The H_I can be written as

$$H_I = \sum_i [U \sum_a n_{ia\uparrow} n_{ia\downarrow} + U' \sum_{\substack{a < b \\ \sigma, \sigma'}} n_{ia\sigma} n_{ib\sigma'} + \sum_{a < b} (J_H \sum_{\sigma, \sigma'} c_{ia\sigma}^{\dagger} c_{ib\sigma'}^{\dagger} c_{ia\sigma'} c_{ib\sigma} + J_{pair} c_{ia\uparrow}^{\dagger} c_{ia\downarrow}^{\dagger} c_{ib\downarrow} c_{ib\uparrow})], \quad (4)$$

where i labels the site of a square lattice, σ, σ' label the spin, and $n_{ia\sigma}$ is number operator at site i of spin σ in orbital a .

Here, we maintain the basic relation $U = U' + 2J_H$, $J_H = J_{pair}$ and set $J_H = \alpha U$ so that U and α are the only two variables in this type of interaction. Throughout this paper, we take eV as the energy unit. In our calculation, we find that the superconducting instability manifests into two pairing states, $d_{x^2-y^2}$ -wave and s_{\pm} -wave, in the parameter space. When $U = 3, \alpha = 0.3$, the system produces $d_{x^2-y^2}$ -wave and when $U = 3, \alpha = 0.6$, the system produces s_{\pm} -wave, the corresponding form factors are shown in Fig.2. More detailed results are listed in Tab.I, where we can see that, when $U \leq 6$, smaller α tends to $d_{x^2-y^2}$ -wave and larger α tends to s_{\pm} -wave, and when $U > 6$, the pairing symmetry maintains to be robust s_{\pm} -wave regardless of the value of J_H . These results are consistent with the previous studies^{18,39,41} where α was taken to be large so that the s_{\pm} -wave was obtained.

IV. EFFECTIVE MAGNETIC EXCHANGE INTERACTIONS

In this section, we address pairing symmetries in a model with effective magnetic exchange interactions. In iron-based superconductors, there are three types of magnetic exchange couplings in an effective model. The first one is the onsite Hund's couplings J_H (see Eq.5).

TABLE I: The pairing symmetry with U, U', J_H, J_{pair} interactions. The parameters satisfy $U = U' + 2J_H, J_H = J_{pair}$ and $J_H = \alpha * U$.

	$\alpha = 0$	$\alpha = 0.1$	$\alpha = 0.2$	$\alpha = 0.3$	$\alpha = 0.4$
$U = 2$	$d_{x^2-y^2}$	$d_{x^2-y^2}$	$s\pm$	$s\pm$	$s\pm$
$U = 3$	$d_{x^2-y^2}$	$d_{x^2-y^2}$	$s\pm$	$s\pm$	$s\pm$
$U = 4$	$d_{x^2-y^2}$	$d_{x^2-y^2}$	$d_{x^2-y^2}$	$s\pm$	$s\pm$
$U = 5$	$d_{x^2-y^2}$	$d_{x^2-y^2}$	$d_{x^2-y^2}$	$s\pm$	$s\pm$
$U = 6$	$d_{x^2-y^2}$	$d_{x^2-y^2}$	$d_{x^2-y^2}$	$s\pm$	$s\pm$
$U = 7$	$s\pm$	$s\pm$	$s\pm$	$s\pm$	$s\pm$
$U = 8$	$s\pm$	$s\pm$	$s\pm$	$s\pm$	$s\pm$

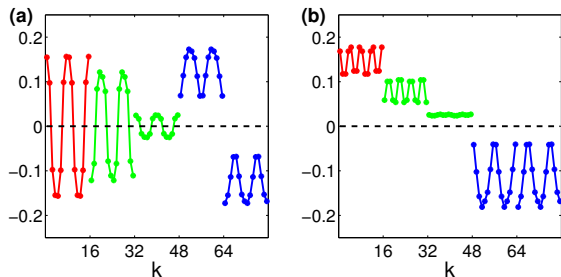


FIG. 2: (color online) The form factor $f_1(k)$ associated to the leading superconducting instability is plotted along the five Fermi surfaces according to the numbering in Fig.1(b). The interaction parameters used in (a) are $U = 3, \alpha = 0.3$, and in (b) are $U = 3, \alpha = 0.6$.

The others are the NN and NNN magnetic exchange couplings, J_1 (see Eq.6) and J_2 (see Eq.7)¹⁰. Taken together, the interaction Hamiltonian can be written as $H_I = H_{J_H} + H_{J_1} + H_{J_2}$ with

$$H_{J_H} = -J_H \sum_i \sum_{a \neq b} \mathbf{S}_{ia} \cdot \mathbf{S}_{ib}, \quad (5)$$

$$H_{J_1} = J_1 \sum_{\langle i,j \rangle} \sum_{a,b} \mathbf{S}_{ia} \cdot \mathbf{S}_{jb}, \quad (6)$$

$$H_{J_2} = J_2 \sum_{\langle\langle i,j \rangle\rangle} \sum_{a,b} \mathbf{S}_{ia} \cdot \mathbf{S}_{jb}, \quad (7)$$

where $\mathbf{S}_{ia} = \frac{1}{2} \sum_{\alpha,\beta} c_{ia\alpha}^\dagger \sigma_{\alpha\beta} c_{ia\beta}$ is the local spin operator, σ is the Pauli matrix, i, j are the lattice sites, α, β are spin indexes, and a, b are orbital indexes.

Then we do Fourier transform $c_{ia}^\dagger = \sum_k c_{ka}^\dagger e^{i\mathbf{k}\mathbf{R}_i}$ and use the relation $\sigma_{\alpha\beta} \cdot \sigma_{\alpha'\beta'} = 2\delta_{\alpha\beta'}\delta_{\beta\alpha'} - \delta_{\alpha\beta}\delta_{\alpha'\beta'}$. Using FRG, as described in the previous section, we study the renormalized interactions described by the four-point vertex associated with the second quantization form in momentum space,

$$\sum_{\substack{k_1, k_2, \\ k_3, k_4}} [V_1(k_1, k_2, k_3, k_4) c_{k_1\alpha}^\dagger c_{k_2b\beta}^\dagger c_{k_4a\beta} c_{k_3b\alpha} + V_2(k_1, k_2, k_3, k_4) c_{k_1\alpha}^\dagger c_{k_2b\beta}^\dagger c_{k_4b\beta} c_{k_3a\alpha}], \quad (8)$$

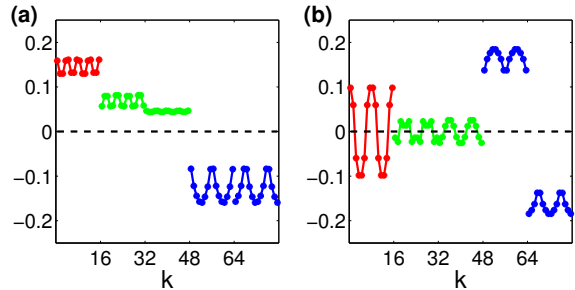


FIG. 3: (color online) (a) The SC form factors for $J_1 = 1.0, J_2 = 1.0, \text{ and } J_H = 0$: the $s\pm$ -wave is robust for $J_2 \gtrsim J_1$. (b) The SC form factor for $J_1 = 3.0, J_2 = 1.0, J_H = 0$: the $d_{x^2-y^2}$ pairing state appears when $J_2 \ll J_1$.

with

$$V_1 = -J_1 (\cos(k_{2x} - k_{3x}) + \cos(k_{2y} - k_{3y})) - 2J_2 \cos(k_{2x} - k_{3x}) \cos(k_{2y} - k_{3y}) + \frac{1}{2} J_H, \quad (9)$$

and

$$V_2 = -\frac{1}{2} J_1 (\cos(k_{1x} - k_{3x}) + \cos(k_{1y} - k_{3y})) - J_2 \cos(k_{1x} - k_{3x}) \cos(k_{1y} - k_{3y}) + \frac{1}{4} J_H, \quad (10)$$

where k_1, k_2, k_3, k_4 denote the momenta of the four particles. Required by the Pauli exclusion principle, $a \neq b$ for the J_H term.

The results are shown in Tab.II and Tab.III with various J_1, J_2 , and AFM J_H values. Through analyzing the results, in this case, we find that the pairing symmetry is largely independent of the J_H values. Between the other two parameters, J_2 plays a more important role than J_1 . It drives a $s\pm$ phase when $J_2 \gtrsim J_1$, shown in Fig.3(a) and a $d_{x^2-y^2}$ state when $J_2 \ll J_1$, shown in Fig.3(b). We note that in Tab.II the $s\pm$ (*nodal*) means that this $s\pm$ -wave has nodes in the small Γ -centered hole pocket. Furthermore, in Tab.III when $J_1 = 1.5, J_2 = 0$ and $J_1 = 2.0, J_2 = 0$, there is a s_{\pm}^h -wave which has a sign change between the $(0,0)$ -centered hole pocket and (π, π) -centered hole pocket or between the two $(0,0)$ -centered hole pockets.

V. THE ORBITAL-DEPENDENT MAGNETIC EXCHANGE INTERACTIONS

For the purpose of studying the interactions with greater depth, we divide the NN AFM J_1 and the NNN AFM J_2 into two parts respectively: the intra-orbital

TABLE II: The pairing symmetry in the presence of the effective NN, NNN and Hund's magnetic exchange couplings.

	$J_2 = 0$				$J_1 = 0$				$J_1 = J_2$			
	$J_1 = 0.5$	$J_1 = 1.0$	$J_1 = 1.5$	$J_1 = 2.0$	$J_2 = 0.5$	$J_2 = 1.0$	$J_2 = 1.5$	$J_2 = 2.0$	$J_1 = 0.5$	$J_1 = 1.0$	$J_1 = 1.5$	$J_1 = 2.0$
$J_H = 0.5$	s_{\pm} (nodal)	s_{\pm} (nodal)	s_{\pm}^h	s_{\pm}^h	s_{\pm}	s_{\pm}	s_{\pm}	s_{\pm}	s_{\pm}	s_{\pm}	s_{\pm}	s_{\pm}
$J_H = 1.0$	s_{\pm}^h	s_{\pm} (nodal)	s_{\pm}^h	s_{\pm}^h	s_{\pm}	s_{\pm}	s_{\pm}	s_{\pm}	s_{\pm}	s_{\pm}	s_{\pm}	s_{\pm}
$J_H = 1.5$	h_{\pm}	s_{\pm} (nodal)	s_{\pm}^h	s_{\pm}^h	s_{\pm}	s_{\pm}	s_{\pm}	s_{\pm}	s_{\pm}	s_{\pm}	s_{\pm}	s_{\pm}
$J_H = 2.0$	h_{\pm}	s_{\pm}^h	s_{\pm}^h	s_{\pm}^h	s_{\pm}	s_{\pm}	s_{\pm}	s_{\pm}	s_{\pm}	s_{\pm}	s_{\pm}	s_{\pm}

TABLE III: The pairing symmetry with only the NN and NNN AFM exchange couplings.

$J_H = 0$	$J_2 = 0$	$J_2 = 0.5$	$J_2 = 1.0$	$J_2 = 1.5$	$J_2 = 2.0$	$J_2 = 2.5$	$J_2 = 3.0$	$J_2 = 3.5$	$J_2 = 4.0$
$J_1 = 0$		s_{\pm}	s_{\pm}	s_{\pm}	s_{\pm}	s_{\pm}	s_{\pm}	s_{\pm}	s_{\pm}
$J_1 = 0.5$	s_{\pm}	s_{\pm}	s_{\pm}	s_{\pm}	s_{\pm}	s_{\pm}	s_{\pm}	s_{\pm}	s_{\pm}
$J_1 = 1.0$	s_{\pm}	s_{\pm}	s_{\pm}	s_{\pm}	s_{\pm}	s_{\pm}	s_{\pm}	s_{\pm}	s_{\pm}
$J_1 = 1.5$	s_{\pm}^h	s_{\pm}	s_{\pm}	s_{\pm}	s_{\pm}	s_{\pm}	s_{\pm}	s_{\pm}	s_{\pm}
$J_1 = 2.0$	s_{\pm}^h	s_{\pm}	s_{\pm}	s_{\pm}	s_{\pm}	s_{\pm}	s_{\pm}	s_{\pm}	s_{\pm}
$J_1 = 2.5$	$d_{x^2-y^2}$	$d_{x^2-y^2}$	s_{\pm}	s_{\pm}	s_{\pm}	s_{\pm}	s_{\pm}	s_{\pm}	s_{\pm}
$J_1 = 3.0$	$d_{x^2-y^2}$	$d_{x^2-y^2}$	$d_{x^2-y^2}$	s_{\pm}	s_{\pm}	s_{\pm}	s_{\pm}	s_{\pm}	s_{\pm}
$J_1 = 3.5$	$d_{x^2-y^2}$	$d_{x^2-y^2}$	$d_{x^2-y^2}$	$d_{x^2-y^2}$	s_{\pm}	s_{\pm}	s_{\pm}	s_{\pm}	s_{\pm}
$J_1 = 4.0$	$d_{x^2-y^2}$	$d_{x^2-y^2}$	$d_{x^2-y^2}$	$d_{x^2-y^2}$	$d_{x^2-y^2}$	s_{\pm}	s_{\pm}	s_{\pm}	s_{\pm}

part and the inter-orbital part. We first study the interaction containing intra-orbital J_1 and inter-orbital J_2 . The initial interaction Hamiltonian is

$$J_1 \sum_{\langle i,j \rangle} \sum_a \mathbf{S}_{ia} \cdot \mathbf{S}_{ja} + J_2 \sum_{\langle\langle i,j \rangle\rangle} \sum_{a \neq b} \mathbf{S}_{ia} \cdot \mathbf{S}_{jb}. \quad (11)$$

This Hamiltonian exhibits a more plentiful pairing phase diagram compared to the full J_1 and J_2 interaction. Varying the intra-orbital J_1 and the inter-orbital J_2 values in the FRG permitted range, we calculate the pairing symmetry numerically and get the phase diagram which is specified in Fig.4.

In the phase diagram, the green-filled region has the s_{\pm} pairing state (the form factor is shown in Fig.5(a)) and the yellow-filled phase in the bottom right corner has d_{xy} symmetry (the form factor is shown in Fig.5(b)). The large-scaled blue-filled phase represents $d_{x^2-y^2}$ symmetry and it is subdivided into three parts which have slightly difference. The form factors of these three $d_{x^2-y^2}$ phases are shown in Fig.6. The red-filled region represents s_{\pm}^h pairing symmetry where intra-orbital J_1 lies in $0 \sim 2.4$ and inter-orbital J_2 lies in $0 \sim 5.5$. In our calculation, we note that there are two s_{\pm}^h phases, the phase labeled by s_{\pm}^h (I) has nodal electron pockets (the form factor is shown in Fig.7(a)) and the region s_{\pm}^h (II) has nodeless electron pockets (the form factor is shown in Fig.7(b)).

Secondly, we take the interactions which contain inter-orbital J_1 and the intra-orbital J_2 . In this case, the in-

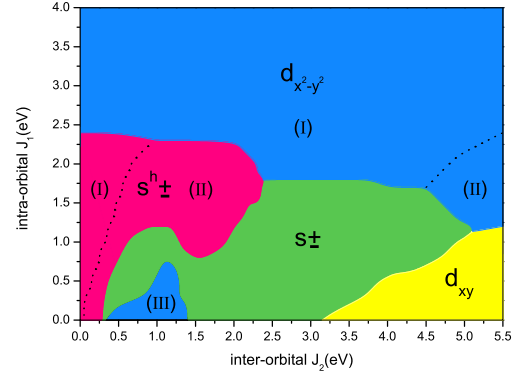


FIG. 4: (color online) The superconducting pairing symmetry phase diagram in the intra-orbital J_1 and inter-orbital J_2 plane. When the interaction parameters vary, there are four different pairing symmetries which are shown by different colors: s_{\pm} -wave (green), d_{xy} -wave (yellow), $d_{x^2-y^2}$ -wave (blue) and s_{\pm}^h -wave (red). The $d_{x^2-y^2}$ -wave has three different form factors and the s_{\pm}^h -wave has two.

teraction part of Hamiltonian is given by

$$J_1 \sum_{\langle i,j \rangle} \sum_{a \neq b} \mathbf{S}_{ia} \cdot \mathbf{S}_{jb} + J_2 \sum_{\langle\langle i,j \rangle\rangle} \sum_a \mathbf{S}_{ia} \cdot \mathbf{S}_{ja}. \quad (12)$$

The result of FRG calculation is summarized in the phase diagram shown in Fig.8. There are three phases in

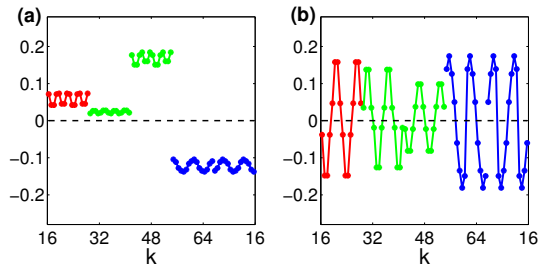


FIG. 5: (color online) The typical SC form factors for s_{\pm} -wave(a) and d_{xy} -wave(b) in the phase diagram Fig.4. The interaction parameters used in (a) are $J_1 = 1.0, J_2 = 2.5$, and in (b) $J_1 = 0.5, J_2 = 5.0$.

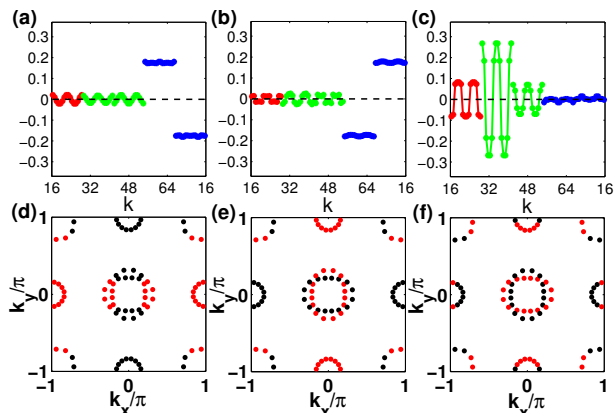


FIG. 6: (color online) The SC form factors(a-c) and the signs of the gap functions(d-e)(the red and black points present opposite sign) for $d_{x^2-y^2}$ -wave in the phase diagram(Fig.4). (a,d)The typical SC form factors and the corresponding signs for the blue (I) region in Fig.4 with $J_1 = 3.0, J_2 = 3.0$. (b,e)The typical SC form factors and the corresponding signs for the blue (II) region in Fig.4 with $J_1 = 1.6, J_2 = 5.0$. (c,f)The typical SC form factor and the corresponding signs for the blue (III) region in Fig.4 with $J_1 = 0.5, J_2 = 1.1$.

the phase diagram in the inter-orbital J_1 and the intra-orbital J_2 plane. When the intra-orbital J_2 is less than 0.5 and the inter-orbital J_1 lies in (0.4, 1.4), it exhibits $d_{x^2-y^2}$ state which is in the blue region. When the intra-orbital J_2 is less than 0.4 and the inter-orbital J_1 is greater than 1.5, it exhibits d_{xy} state, as shown in the yellow region in Fig.8. The remaining green region in Fig.8 represents s_{\pm} state.

VI. DISCUSSION AND SUMMARY

From our calculations, it is clear that the results of FRG on superconducting pairing symmetries greatly depend on the initial interactions. Even in a fixed Fermi surface topology which was largely acknowledged to host a s_{\pm} -wave in the previous studies, a small variation of

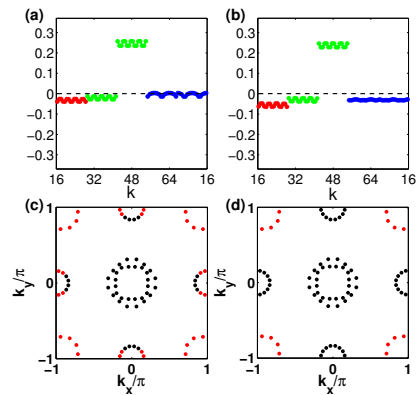


FIG. 7: (color online) The SC form factors(a-c) and the signs(d-e) for the s_{\pm}^h -wave in the phase diagram(Fig.4). (a,c)The typical SC form factors and the corresponding signs for the red (I) region in Fig.4 with $J_1 = 1.5, J_2 = 0.3$. (b,d)The typical SC form factors and the corresponding signs for the red (II) region in Fig.4 with $J_1 = 2.0, J_2 = 1.5$.

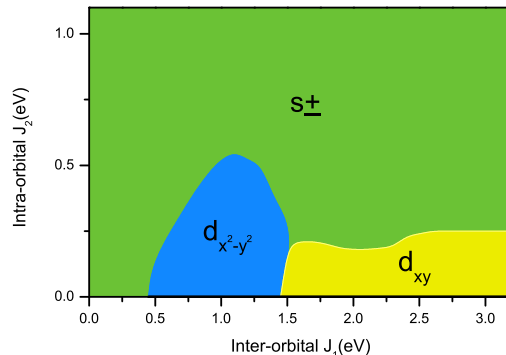


FIG. 8: (color online)The superconducting pairing symmetry phase diagram in the inter-orbital J_1 and intra-orbital J_2 plane. There are three different pairing symmetry states: s_{\pm} -wave, $d_{x^2-y^2}$ -wave and d_{xy} -wave.

interaction parameters can lead to other pairing symmetries and result in a complicated phase diagram. These results essentially suggest that the FRG method lacks predicting power for complex systems such as iron-based superconductors since it is difficult to extract an accurate effective model with precise estimation of interaction parameters.

Nevertheless, robust results can be observed in our FRG results. Firstly, the intra-orbital interaction is generally more important than the inter-orbital interaction in determining pairing symmetries. Once the intra-orbital interactions are large enough, the pairing symmetry appears to be rather robust. Secondly, in general, the large NN intra-orbital AFM exchange coupling favors a $d_{x^2-y^2}$ -wave and the large NNN intra-orbital AFM favors a s_{\pm} -wave. Other pairing symmetries become possible only when the intra-orbital magnetic exchange couplings

are small. Finally, the fact that only the $d_{x^2-y^2}$ -wave and the $s\pm$ -wave are obtained in the model with onsite repulsive interactions suggests that the low energy effective magnetic exchange interactions induced by the onsite repulsive interactions can be approximated to an intra-orbital $J_1 - J_2$ model.

As experimentally, s -wave pairing symmetry is rather robust throughout different families of iron-based superconductors⁴², the consistency between the experimental and FRG results clearly suggests that the intra-orbital AFM exchange coupling J_2 must be the dominant source for superconducting pairing. Thus, it is likely that the NN repulsive interactions must be important in iron-based superconductors as it has been recently pointed out that it can stabilize the extended s -wave pairing by suppressing the pairing channel caused by the NN AFM

exchange coupling J_1 .

In summary, we have revisited the FRG results on pairing symmetries in iron-based superconductors. We show that even with a fixed Fermi surface topology, which previously was considered to support $s\pm$ -wave, different emergent pairing channels can be easily induced by varying interaction parameters. The results suggest an accurate effective model has to be built before FRG can help to predict pairing symmetries.

Acknowledgement: The work is supported by the Ministry of Science and Technology of China 973 program (No. 2015CB921300), National Science Foundation of China (Grant No. NSFC-1190020, 11334012), and the Strategic Priority Research Program of CAS (Grant No. XDB07000000).

-
- ¹ Y. Kamihara, T. Watanabe, M. Hirano, and H. Hosono, *J. Am. Chem. Soc.* **130**, 3296 (2008).
² P. J. Hirschfeld, M. M. Korshunov, and I. I. Mazin, *Rep. Prog. Phys.* **74**, 124508 (2011).
³ C. Andrey, *Annu. Rev. Condens. Matt. Phys.* **3**, 57 (2012).
⁴ D. J. Scalapino, *Rev. Mod. Phys.* **84**, 1383 (2012).
⁵ P. M. Aswathy, J. B. Anooja, P. M. Sarun, and U. Syamaprasad, *Supercond. Sci. Tech.* **23**, 073001 (2010).
⁶ G. R. Stewart, *Rev. Mod. Phys.* **83**, 1589 (2011).
⁷ D. C. Johnston, *Adv. Phys.* **59**, 803 (2010).
⁸ P. Richard, T. Qian, and H. Ding, arXiv: 1503.07269 (2015).
⁹ I. I. Mazin, D. J. Singh, M. D. Johannes, and M. H. Du, *Phys. Rev. Lett.* **101**, 057003 (2008).
¹⁰ K. Seo, B. Bernevig, and J. P. Hu, *Phys. Rev. Lett.* **101**, 206404 (2008).
¹¹ K. Kuroki *et al.*, *Phys. Rev. Lett.* **101**, 087004 (2008).
¹² J. Guo *et al.*, *Phys. Rev. B* **82**, 180520 (2010).
¹³ Y. Zhang *et al.*, *Nature Mater.* **10**, 273 (2011).
¹⁴ D. Liu *et al.*, *Nature Commun.* **3**, 931 (2012).
¹⁵ T. Sato *et al.*, *Phys. Rev. Lett.* **103**, 047002 (2009).
¹⁶ T. Yoshida *et al.*, *J. Phys. Chem. Solids* **72**, 465 (2011).
¹⁷ J. P. Reid *et al.*, *Phys. Rev. Lett.* **109**, 087001 (2012).
¹⁸ R. Thomale *et al.*, *Phys. Rev. Lett.* **107**, 117001 (2011).
¹⁹ S. Maiti *et al.*, *Phys. Rev. B* **84**, 224505 (2011).
²⁰ S. Maiti, M. M. Korshunov, and A. V. Chubukov, *Phys. Rev. B* **85**, 014511 (2012).
²¹ J. P. Hu and N. N. Hao, *Phys. Rev. X* **2**, 021009 (2012).
²² Z. P. Yin, K. Haule, and G. Kotliar, *Nature Phys.* **10**, 845 (2014).
²³ F. F. Tafti *et al.*, *Nature Phys.* **9**, 349 (2013).
²⁴ D. Watanabe *et al.*, *Phys. Rev. B* **89**, 115112 (2014).
²⁵ J. P. Hu, *Phys. Rev. X* **3**, 031004 (2013).
²⁶ M. Khodas and A. Chubukov, *Phys. Rev. Lett.* **108**, 247003 (2012).
²⁷ C. Platt *et al.*, *Phys. Rev. B* **85**, 180502 (2012).
²⁸ S. Maiti and A. V. Chubukov, *Phys. Rev. B* **87**, 144511 (2013).
²⁹ M. Marciani, L. Fanfarillo, C. Castellani, and L. Benfatto, *Phys. Rev. B* **88**, 214508 (2013).
³⁰ R. Shankar, *Rev. Mod. Phys.* **66**, (1994).
³¹ W. Metzner *et al.*, *Rev. Mod. Phys.* **84**, 299 (2012).
³² C. Platt, W. Hanke, and R. Thomale, *Adv. Phys.* **62**, 453 (2013).
³³ C. Honerkamp, *Eur. Phys. J. Spec. Top.* **188**, 33 (2010).
³⁴ F. Wang, H. Zhai, and D.H. Lee, *Eur. Phys. Lett.* **85**, 37005 (2009).
³⁵ S. Graser *et al.*, *Phys. Rev. B* **81**, 214503 (2010).
³⁶ D. Zanchi and H. Schulz J, *Phys. Rev. B* **61**, 13609 (2000).
³⁷ R. Thomale, C. Platt, J. P. Hu, C. Honerkamp, and B. A. Bernevig, *Phys. Rev. B* **80**, 180505 (2009).
³⁸ C. Honerkamp, M. Salmhofer, N. Furukawa, and T. Rice, *Phys. Rev. B* **63**, 18 (2001).
³⁹ F. Wang *et al.*, *Phys. Rev. Lett.* **102**, 047005 (2009).
⁴⁰ J. Yuan and J. P. Hu, arXiv: 1403.6240 (2014).
⁴¹ R. Thomale, C. Platt, W. Hanke, C. Honerkamp, and B. A. Bernevig, *Phys. Rev. Lett.* **106**, 187003 (2011).
⁴² J. P. Hu and J. Yuan, arXiv: 1506.05791v1 (2015).